Enhancing the Chemical Flexibility of Hybrid Perovskites by Introducing Divalent Ligands

Lydia G. Burley,[a] James Beecham-Lonsdale,[a] Anant Kumar Srivastava,[a,b] Ines E. Collings,[c] and Paul J. Saines*[a]

[a] School of Physical Sciences, University of Kent, Canterbury, Kent, CT2 7NH, United Kingdom

[b] Department of Materials Engineering, Indian Institute of Science (IISc), Bangalore-560012, Karnataka, India

[c] Centre for X-ray Analytics, Empa – Swiss Federal Laboratories for Materials Science and Technology, 8600, Dübendorf, Switzerland

* Corresponding Author Email Address: P.Saines@kent.ac.uk

Electronic Supplementary Information (ESI)

Synthesis

The two compounds reported in this work, $[(CH_3)_2NH_2]Er(HCO_2)_2(C_2O_4)$ and $[(NH_2)_3C]Er(HCO_2)_2(C_2O_4)$, were both made by solvothermal synthesis using a 23 mL autoclave containing 6 mL of a 1:1 ratio of deionised water:N,N-dimethlyformamide (99 % Fisher Scientific). A high quality sample of $[(CH_3)_2NH_2]Er(HCO_2)_2(C_2O_4)$ was made via a seven day reaction at 100 °C using $Er(NO_3)_3{\cdot}5H_2O$ (0.4432 g, 1 mmol, 99.9 % Acros Organics), dimethylamine (3 mmol, 33 wt % in ethanol, Sigma Aldrich), oxalic acid (0.0902 g, 1 mmol, 98 %, Acros Organics) and sodium carbonate (0.0210 g, 0.2 mmol, 99.5 %, Acros Organics). The formate is generated in-situ by decomposition of dimethylformamide, which also produces additional dimethylammonium. $[(NH_2)_3C]Er(HCO_2)_2(C_2O_4)$ was made using a similar method via a three day reaction but with the use of guanidinum carbonate (0.0903 g, 3 mmol, 99 % Acros Organics) instead of dimethylamine. Despite the anticipated presence of $[(CH_3)_2NH_2]^+$ in the reaction mixture used in the synthesis of $[(NH_2)_3C]Er(HCO_2)_2(C_2O_4)$ due to the decomposition of dimethylformamide there was no indication of $[(CH_3)_2NH_2]^+$ in the sample. Both reactions yield pale pink crystals with 77 % and 97 % yields, with respect to Er, for $[(CH_3)_2NH_2]Er(HCO_2)_2(C_2O_4)$ and $[(NH_2)_3C]Er(HCO_2)_2(C_2O_4)$, respectively.

Structure Determination

Crystal structure determination was carried out using a dual source Rigaku Oxford Diffraction Supernova equipped with Mo K_α and CuK_α micro-focus sources (50 kV, 0.80 mA) with multi-layered optics and an Atlas S2 CCD detector. An Oxford Cryosystems cryostream was used to control the temperature at which the sample was held with samples mounted on MiTeGen microloops for measurements below ambient temperature or a glass rod, above amient temperature. Data were integrated and absorption correction performed using the CrysAlisPro software suite.[1] Structures were solved using direct methods in SHELXT[2] or charge flipping methods in olex.2,[3] with least-squares refinements carried out using SHELXL-2014[4] via the Olex2 graphical user interface[5]. Displacement parameters of non-hydrogen atoms were refined anisotropically and hydrogen atom position located geometrically using the AFIX commands in SHELX-2014,[4] with their displacement parameters constrained to 1.2 or 1.5 times the carbon or nitrogen atoms they were connected to, respectively (see Table S1 for crystallographic details). Attempts were made to collect data on $[(CH_3)_2NH_2]Er(HCO_2)_2(C_2O_4)$ below 170 K, which led to the crystal splitting. This led to serious degradation of the quality of the structures obtained at these temperatures although there was no indication of any phase transitions observed. For $[(NH_2)_3C]Er(HCO_2)_2(C_2O_4)$ a modest reduction in the data quality was observed at 500 K, possibly due to the loss of some degree of crystallinity although whether this is due to heating or prolonged exposure to the X-ray beam is unclear, regardless the cation remains clearly ordered at this temperature.

Table S1: Crystallographic Data for $[(CH_3)_2NH_2]Er(HCO_2)_2(C_2O_4)$ and $[(NH_2)_3C]Er(HCO_2)_2(C_2O_4)$ determined using single crystal X-ray diffraction using Mo and Cu K_α radiation, respectively.

Compound	**$[(CH_3)_2NH_2]Er(HCO_2)_2(C_2O_4)$**	**$[(CH_3)_2NH_2]Er(HCO_2)_2(C_2O_4)$**	**$[(CH_3)_2NH_2]Er(HCO_2)_2(C_2O_4)$**	**$[(NH_2)_3C]Er(HCO_2)_2(C_2O_4)$**	**$[(NH_2)_3C]Er(HCO_2)_2(C_2O_4)$**	**$[(NH_2)_3C]Er(HCO_2)_2(C_2O_4)$**
Formula	$C_6H_{10}ErNO_8$	$C_6H_{10}ErNO_8$	$C_6H_{10}ErNO_8$	$C_5H_8ErN_3O_8$	$C_5H_8ErN_3O_8$	$C_5H_8ErN_3O_8$
Formula Weight	391.41	391.41	391.41	405.39	405.39	405.39
T (K)	170(2)	293(2)	500(2)	100(2)	310(2)	460(2)
Crystal System	Monoclinic	Monoclinic	Monoclinic	Orthorhombic	Orthorhombic	Orthorhombic
Space Group	*P*2/*n* (13)	*P*2/*n* (13)	*P*2/*n* (13)	*Pcca* (54)	*Pcca* (54)	*Pcca* (54)
a (Å)	9.1654(3)	9.1700(4)	9.1445(5)	8.3846(3)	8.4795(4)	8.5549(7)
b (Å)	8.9841(2)	8.9919(3)	9.0168(4)	6.5898(2)	6.6014(2)	6.6144(4)
c (Å)	13.1605(4)	13.1900(6)	13.2244(7)	19.4181(5)	19.2633(5)	19.1726(7)
α (°)	90	90	90	90	90	90
β (°)	97.185(2)	96.851(4)	96.821(5)	90	90	90
γ (°)	90	90	90	90	90	90
V (Å^3)	1075.16(5)	1079.83(8)	1082.69(10)	1072.91(6)	1078.28(7)	1084.89(12)
Z	4	4	4	4	4	4
ρ_{calc} (g cm^{-3})	2.418	2.408	2.401	2.510	2.497	2.482
μ (cm^{-1})	7.833	7.799	7.779	14.952	14.878	14.787
Refl. Meas./Unique	9990/2744 [R_{int} = 0.0861]	9202/2658 [R_{int} = 0.1051]	10228/2743 [R_{int} = 0.0286]	3266/1038 [R_{int} = 0.0664]	3290/ 1045 [R_{int} = 0.0607]	3323 / 1033 [R_{int} = 0.404]
Parameters Refined	148	148	148	80	80	80
*R*1, *wR*2[a] (all)	0.0376, 0.0838	0.0343, 0.0715	0.0271, 0.0557	0.0938, 0.2147	0.0970, 0.2222	0.1023, 0.2097
*R*1, *wR*2[a] (obs)	0.0326, 0.0811	0.0315, 0.0697	0.0234, 0.0538	0.0828, 0.1975	0.0829, 0.1959	0.0806, 0.1864
χ^2	1.061	1.068	1.058	1.046	1.023	1.106

[a] $w = 1/\left[\sigma^2\left(F_o^2\right) + (aP)^2 + bP\right]$ and $P = (\max\left(F_0^2,0\right) + 2F_c^2)/3$; $R1 = \sum||F_o| - |F_c||/\sum|F_o|$ and $wR_2 = \sqrt{\left[\left(F_0^2 - F_c^2\right)^2/\sum w\left(F_o^2\right)^2\right]}$

Table S2: Cation coordination distances in Å at 293 K for $[(CH_3)_2NH_2]Er(HCO_2)_2(C_2O_4)$ or 310 K for $[(NH_2)_3C]Er(HCO_2)_2(C_2O_4)$.

$[(CH_3)_2NH_2]Er(HCO_2)_2(C_2O_4)$		**$[(NH_2)_3C]Er(HCO_2)_2(C_2O_4)$**	
Er1-O4	2 × 2.279(3)	Er1-O2	2 x 2.242(10)
Er1-O7	2 × 2.350(3)	Er1-O1	2 x 2.342(9)
Er1-O1	2 × 2.363(3)	Er1-O4	2 x 2.379(8)
Er1-O8	2 × 2.388(3)	Er1-O3	2 x 2.390(8)
Er2-O3	2 × 2.294(4)		
Er2-O2	2 × 2.326(3)		
Er2-O6	2 × 2.358(3)		
Er2-O5	2 × 2.390(3)		

Table S3: Cation coordination bond angles in ° at 293 K for $[(CH_3)_2NH_2]Er(HCO_2)_2(C_2O_4)$ or 310 K for $[(NH_2)_3C]Er(HCO_2)_2(C_2O_4)$.

	$[(CH_3)_2NH_2]Er(HCO_2)_2(C_2O_4)$			$[(NH_2)_3C]Er(HCO_2)_2(C_2O_4)$	
O7-Er1-O8	2 × 67.99(10)	O5-Er2-O6	2 × 68.09(10)	O4-Er1-O3	2 x 67.8(3)
O1-Er1-O4	2 × 70.88(12)	O3-Er2-O5	2 × 70.53(14)	O2-Er1-O3	2 x 73.4(4)
O1-Er1-O8	2 × 74.31(11)	O2-Er2-O3	2 × 74.23(13)	O1-Er1-O3	2 x 74.3(3)
O1-Er1-O7	2 × 75.19(11)	O2-Er2-O3	2 × 74.86(13)	O2-Er1-O1	2 x 75.6(3)
O4-Er1-O8	2 × 76.20(13)	O2-Er2-O6	2 × 77.08(11)	O4-Er1-O4	2 x 76.2(4)
O4-Er1-O4	78.1(2)	O2-Er2-O5	2 × 78.18(12)	O2-Er1-O1	2 x 76.5(3)
O1-Er1-O4	2 × 80.37(12)	O5-Er2-O6	2 × 79.57(12)	O4-Er1-O3	2 x 77.3(3)
O7-Er1-O7	81.23(18)	O6-Er2-O6	80.38(16)	O1-Er1-O4	2 x 77.5(3)
O7-Er-O8	2 × 82.22(12)	O3-Er2-O3	88.1(2)	O2-Er1-O4	2 x 109.0(4)
O4-Er1-O7	2 × 107.73(14)	O3-Er2-O6	2 × 107.85(14)	O1-Er1-O3	2 x 121.5(3)
O1-Er1-O8	2 × 118.98(12)	O2-Er2-O5	2 × 118.28(13)	O3-Er1-O3	2 x 135.3(4)
O1-Er1-O7	2 × 137.68(11)	O2-Er2-O2	136.49(16)	O1-Er1-O4	2 x 137.5(3)
O4-Er1-O8	2 × 139.49(11)	O5-Er2-O5	137.47(17)	O2-Er1-O4	2 x 145.0(3)
O8-Er1-O8	140.73(16)	O2-Er2-O6	2 × 142.18(11)	O2-Er1-O3	2 x 147.0(3)
O1-Er1-O1	142.83(16)	O3-Er2-O6	2 × 142.35(12)		
O4-Er-O7	2 × 150.95(12)	O3-Er2-O5	2 × 148.71(13)		

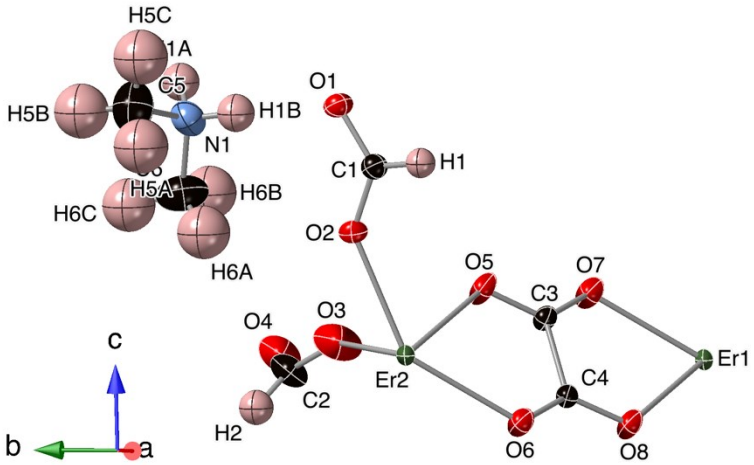

Fig. S1: Depiction of the asymmetric unit of $[(CH_3)_2NH_2]Er(HCO_2)_2(C_2O_4)$ at 293 K with atoms shown as thermal ellipsoids with a 50 % probability distribution. Colours are the same as shown in Fig. 1.

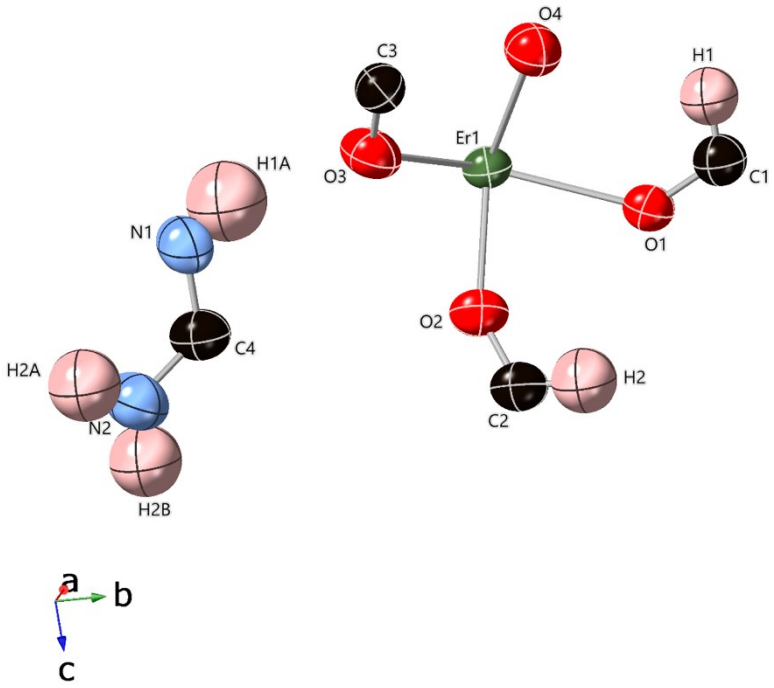

Fig. S2: Depiction of the asymmetric unit of $[(CH_2)_3N]Er(HCO_2)_2(C_2O_4)$ at 310 K with atoms shown as thermal ellipsoids with a 50 % probability distribution. Colours are the same as shown in Fig. 1.

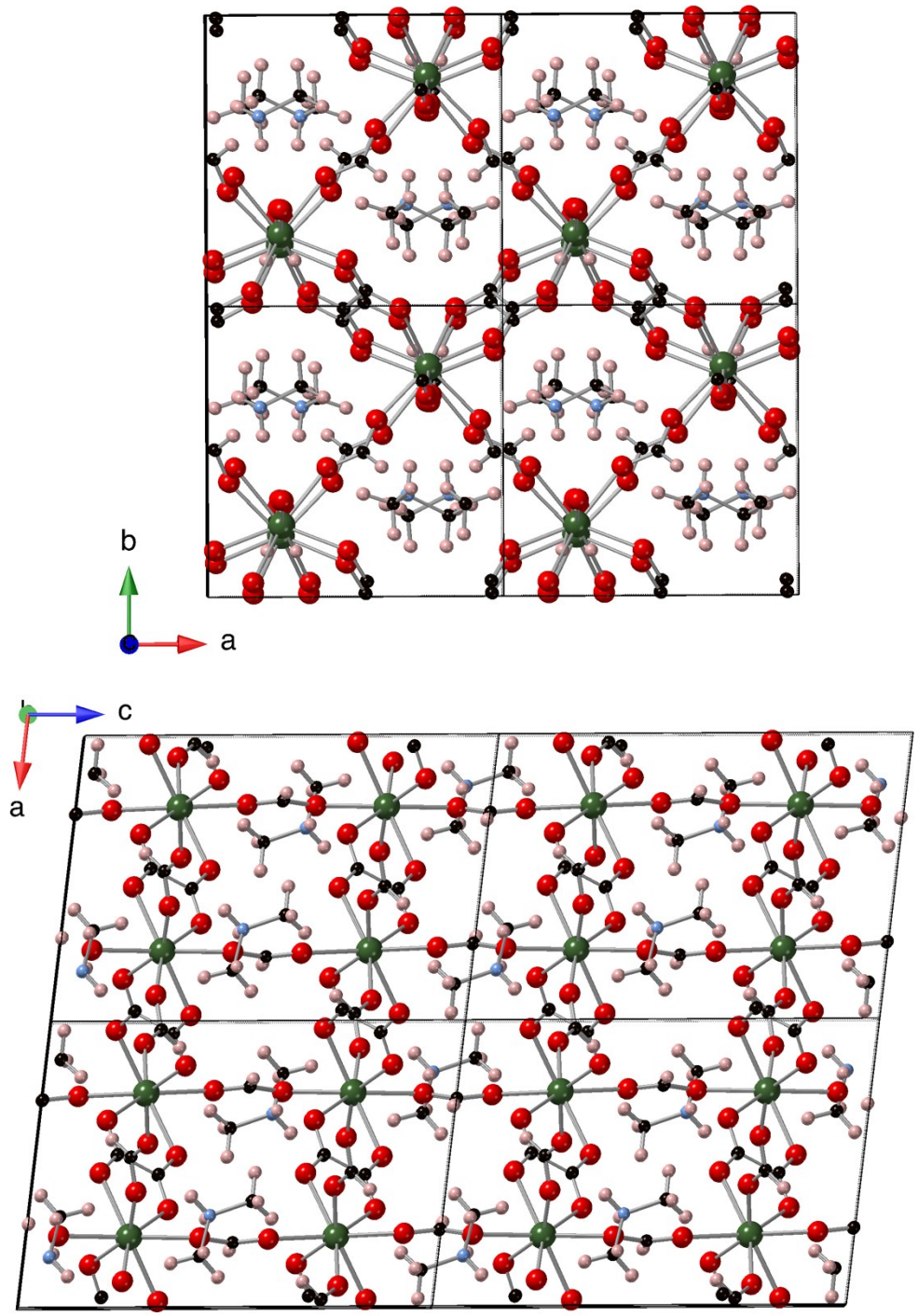

Fig. S3: Depiction of a 2 × 2 × 2 multiple of the unit cell of $[(CH_3)_2NH_2]Er(HCO_2)_2(C_2O_4)$. Colours of atoms are as in Fig. 1.

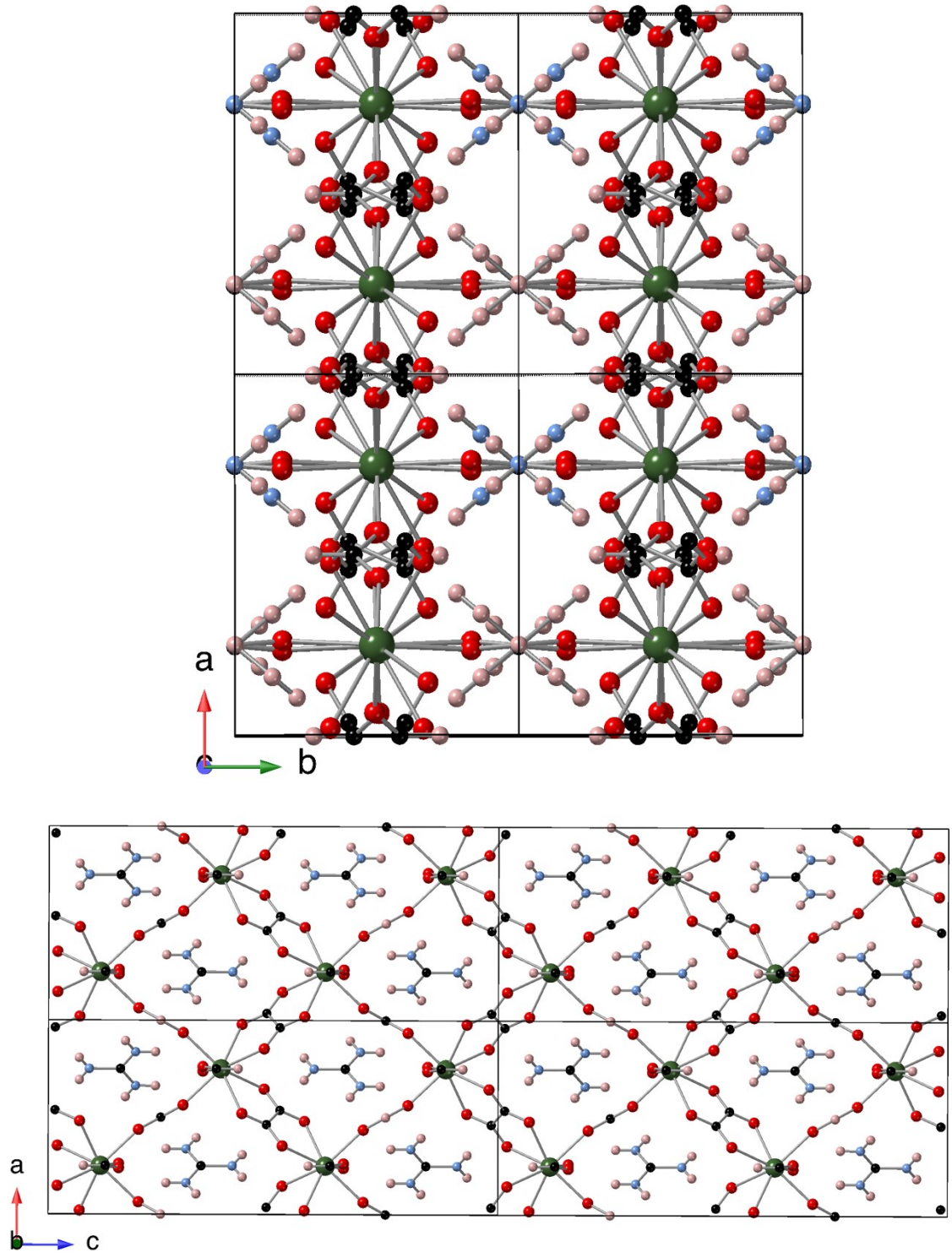

Fig. S4: Depiction of a 2 × 2 × 2 multiple of the unit cell of $[(NH_2)_3C]Er(HCO_2)_2(C_2O_4)$. Colours of atoms are as in Fig. 1.

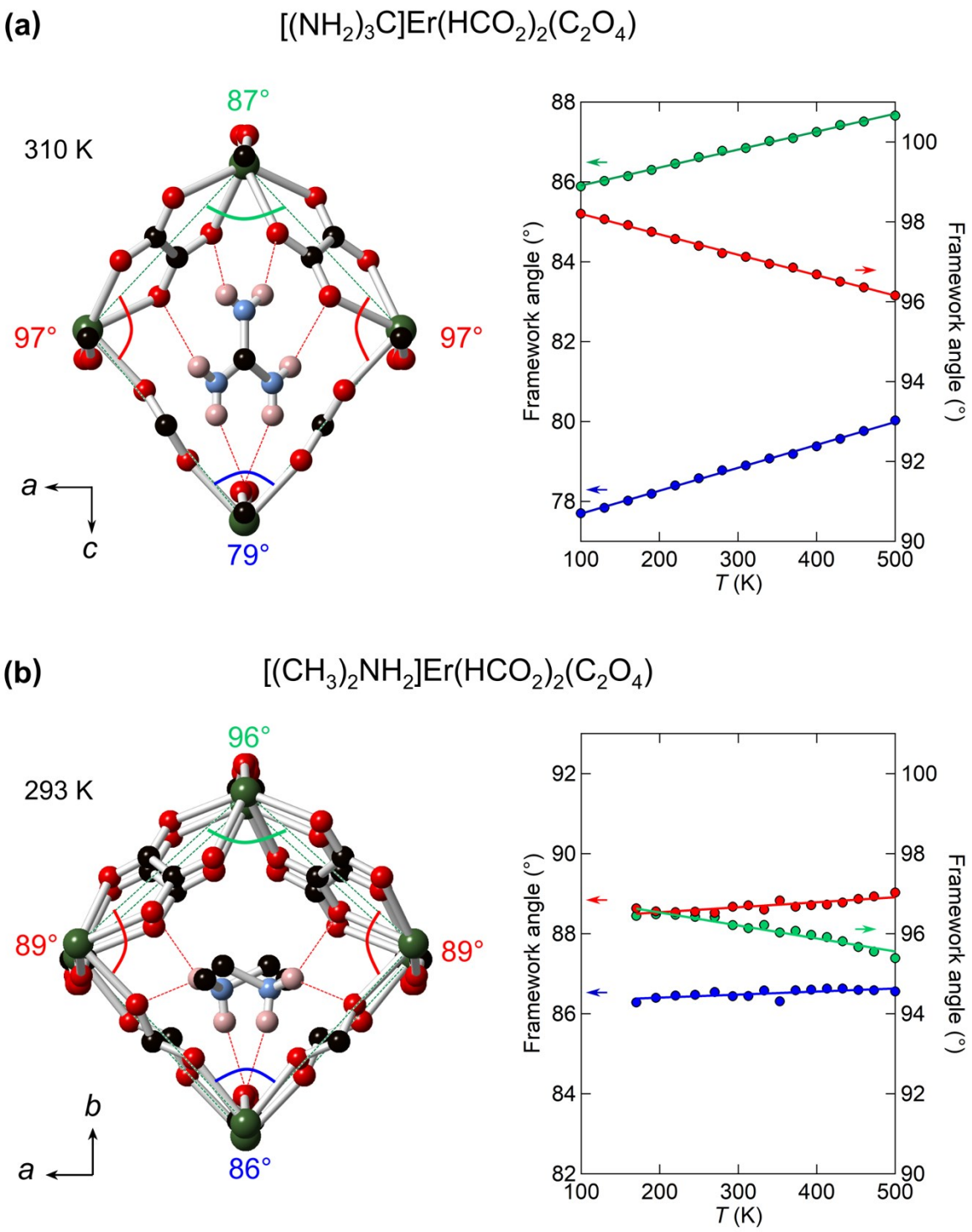

Fig. S5: Framework pores of (a) $[(NH_2)_3C][Er(HCO_2)_2(C_2O_2)$ at 310 K and (b) $[(CH_3)_2NH_2][Er(HCO_2)_2(C_2O_2)$ at 293 K and with the corresponding variable-temperature framework angles. The atomic colours indicate dark green for Er, red for O, black for C, blue for N, and pink for H. Only the hydrogens from the NH_2 groups are shown for clarity. Hydrogen bonding interactions are indicated by dotted red lines, and connected Er ions are indicated with dotted green lines, with the corresponding framework angles.

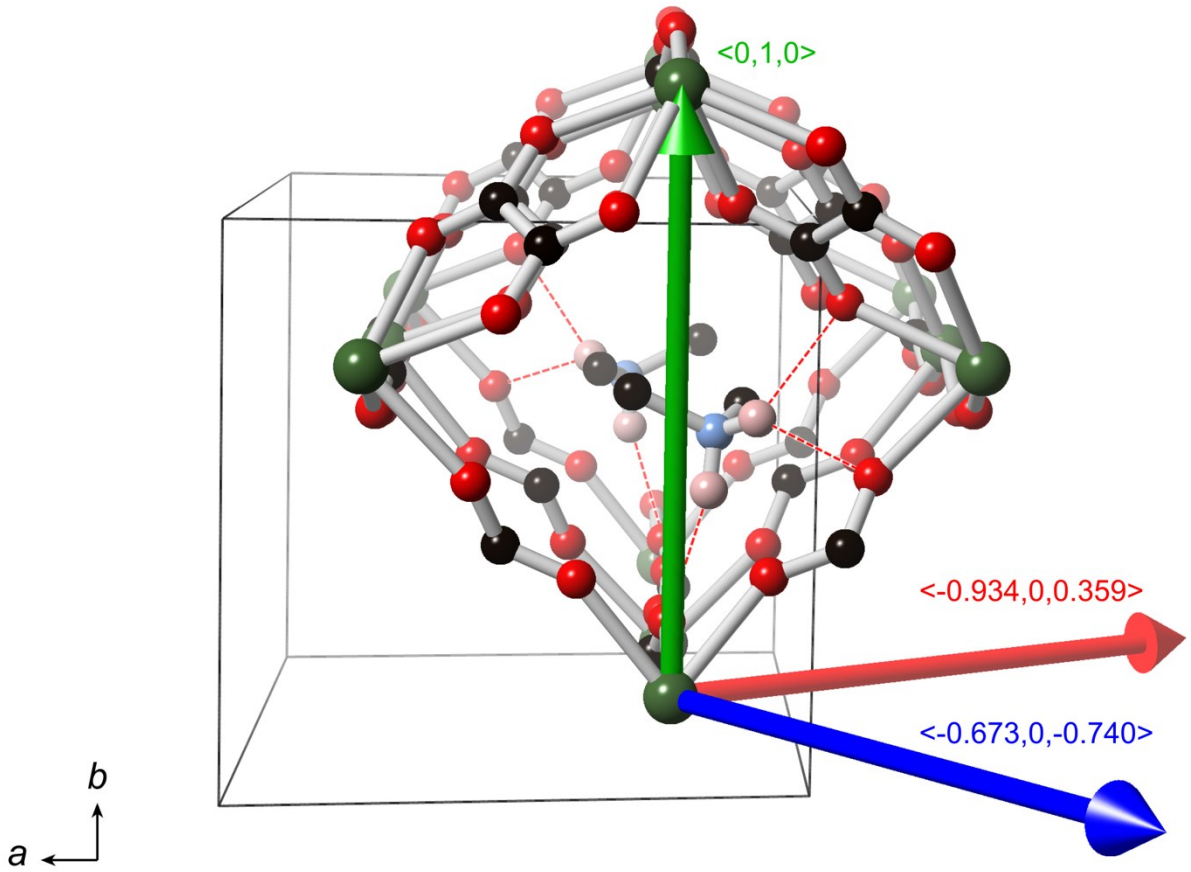

Fig. S6: Principal axes for thermal expansion of $[(NH_2)_3C]Er(HCO_2)_2(C_2O_4)$ shown with reference to the framework pore of the crystal structure.

Bulk Composition

Powder X-ray diffraction was performed using a Rigaku Miniflex diffractometer with a D/teX Ultra detector operating in Bragg-Brentano geometry with the sample held on a zero background Si wafer plate; both of these diffractometers used Cu K_α radiation operating at 40 kV and either 15 mA or 40 mA for the Miniflex and X'Pert[3], respectively. Data were fitted using the Le Bail method in the programme Rietica v4.0[6] using a pseudo-Voigt profile peak shape with Finger-Cox-Jephcoat (FCJ) peak asymmetry (see Fig. S3 & S4).

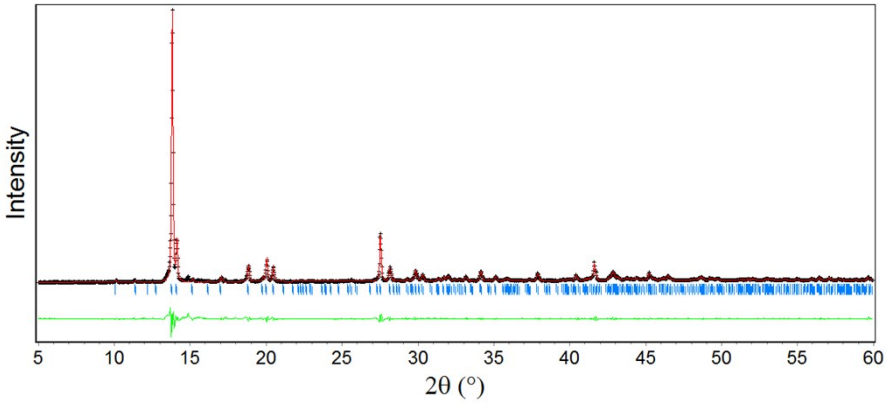

Fig. S7: Le Bail fit to the diffraction pattern of $[(CH_3)_2NH_2]Er(HCO_2)_2(C_2O_4)$. Observed, calculated and difference intensities are shown as black crosses, red continuous lines and green continuous lines, respectively, with expected Bragg peaks indicated by vertical blue markers. R_p = 5.72 %, R_{wp} = 9.16% and χ^2 = 9.10. *a* = 9.1708(5) Å, *b* = 8.9866(4) Å, *c* = 13.1708(6) Å, β = 96.949(5)° and volume = 1077.48(9) Å^3.

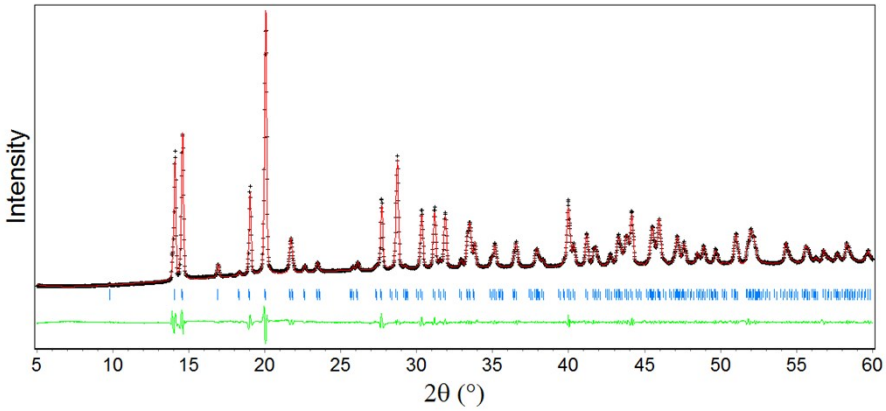

Fig. S8: Le Bail fit to the diffraction pattern of $[(CH_2)_3N]Er(HCO_2)_2(C_2O_4)$. Observed, calculated and difference intensities are shown as black crosses, red continuous lines and green continuous lines, respectively, with expected Bragg peaks indicated by vertical blue markers. R_p = 2.72%, R_{wp} = 4.18 % and χ^2 = 15.7. *a* = 8.4607(3) Å, *b* = 6.60859(16) Å, *c* = 19.3541(5) Å and volume 1082.16(5) Å^3.

Thermal Analysis and Infrared Spectroscopy

Thermal analysis was carried out using a NETZSCH 409 PG/PC TGA capable of simultaneous thermogravimetric analysis (TGA) and differential scanning calorimetry (DSC). The sample was held in a ceramic crucible under nitrogen or air and heated at a rate of 10 K/min. Infrared spectra were measured over a range of 500-4000 cm^{-1} using a Shimadzu IRAffinity-1S Fourier Transform Spectrometer equipped with an attenuated total reflection stage. Measurements were averaged over 32 scans with a resolution of 4 cm^{-1}.

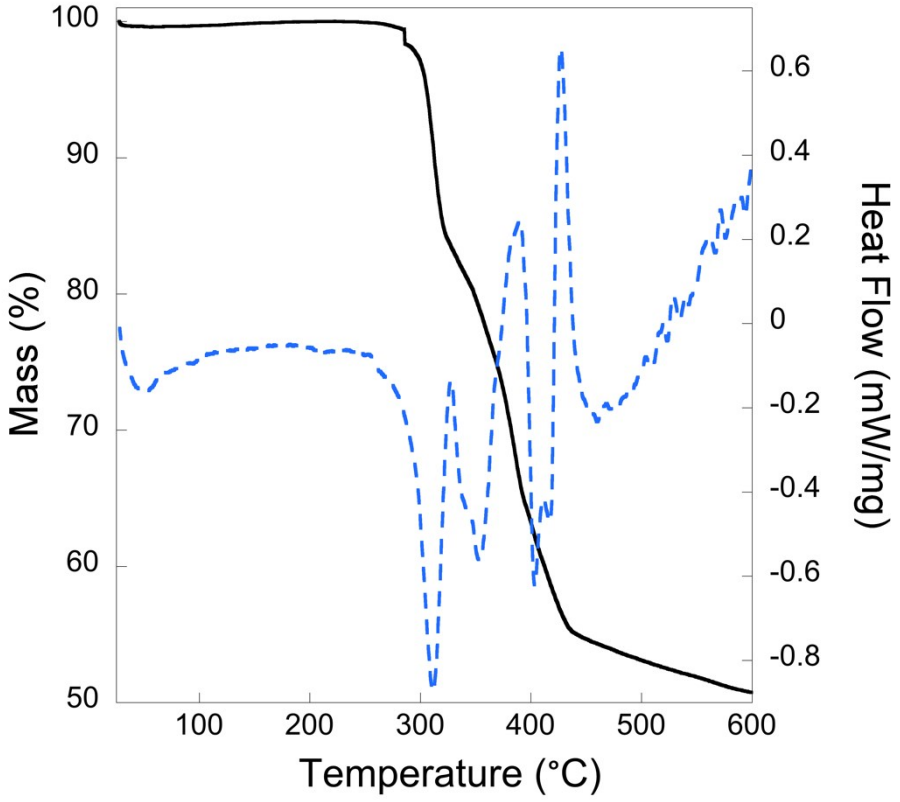

Fig. S9: Thermogravimetric (continuous black line) and differential thermal (dotted blue line) analysis obtained from $[(CH_3)_2NH_2]Er(HCO_2)_2(C_2O_4)$ in N_2.

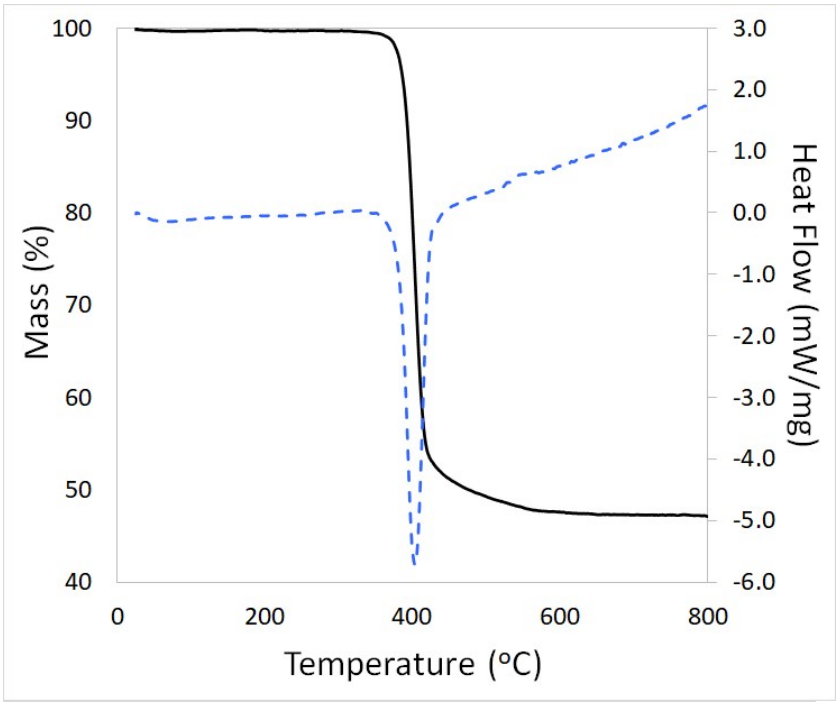

Fig. S10: Thermogravimetric (continuous black line) and differential thermal (dotted blue line) analysis obtained from $[(NH_2)_3C]Er(HCO_2)_2(C_2O_4)$ in N_2.

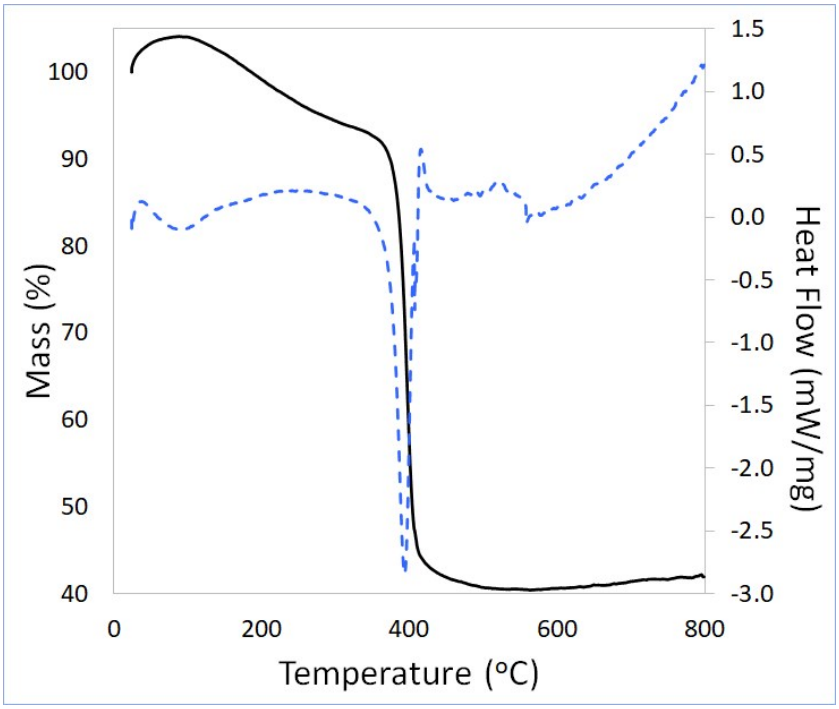

Fig. S11: Thermogravimetric (continuous black line) and differential thermal (dotted blue line) analysis obtained from $[(NH_2)_3C]Er(HCO_2)_2(C_2O_4)$ in air.

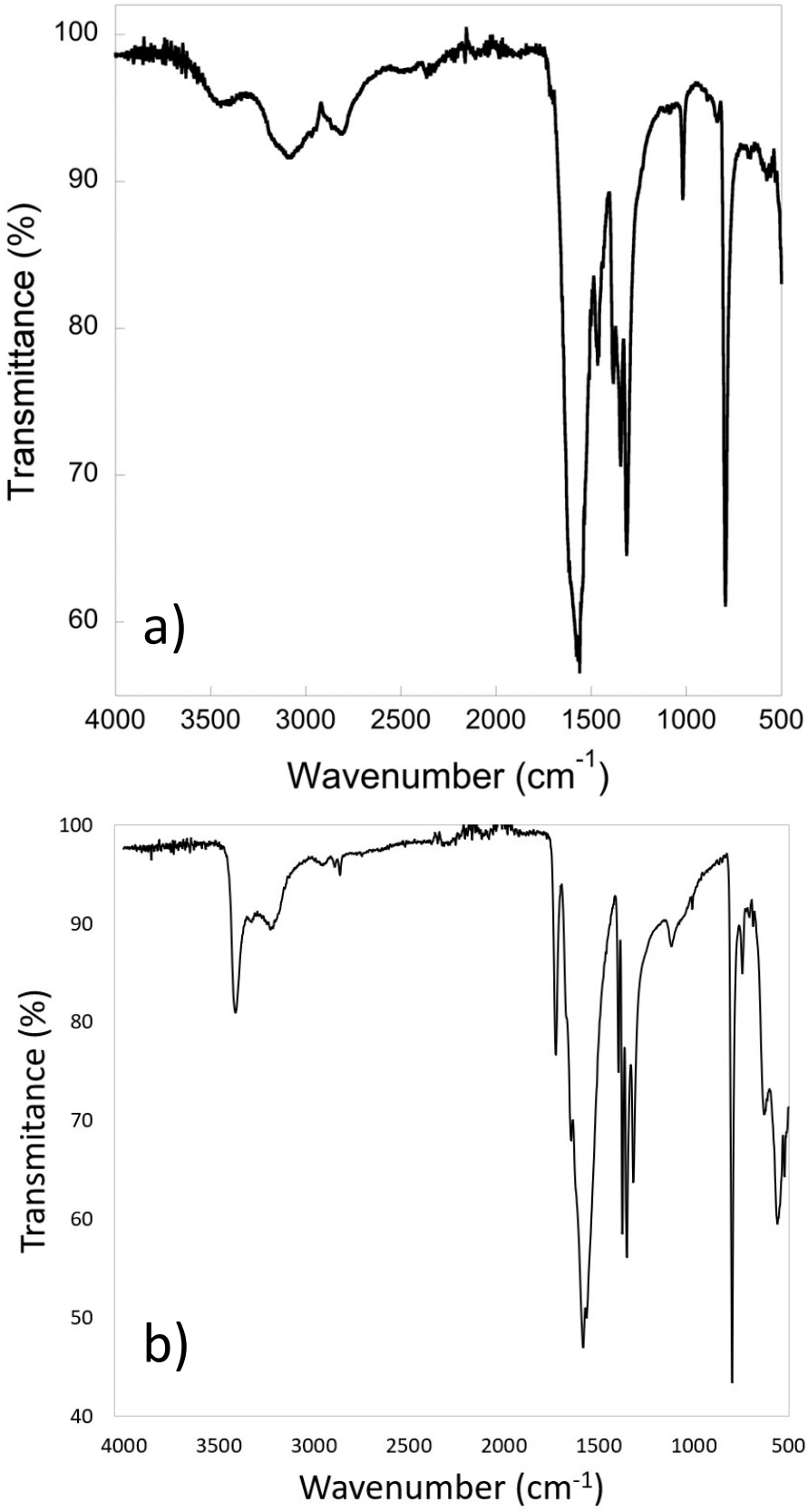

Fig. S12: Infrared spectra of a) $[(CH_3)_2NH_2]Er(HCO_2)_2(C_2O_4)$ and b) $[(NH_2)_3C]Er(HCO_2)_2(C_2O_4)$.

Magnetic Property Measurements

Magnetic Property measurements of $[(CH_3)_2NH_2]Er(HCO_2)_2(C_2O_4)$ were carried out using a Quantum Design Magnetic Property Measurement System (MPMS) equipped with a 7 T magnet with the sample held in a straw with a uniform diamagnetic background.

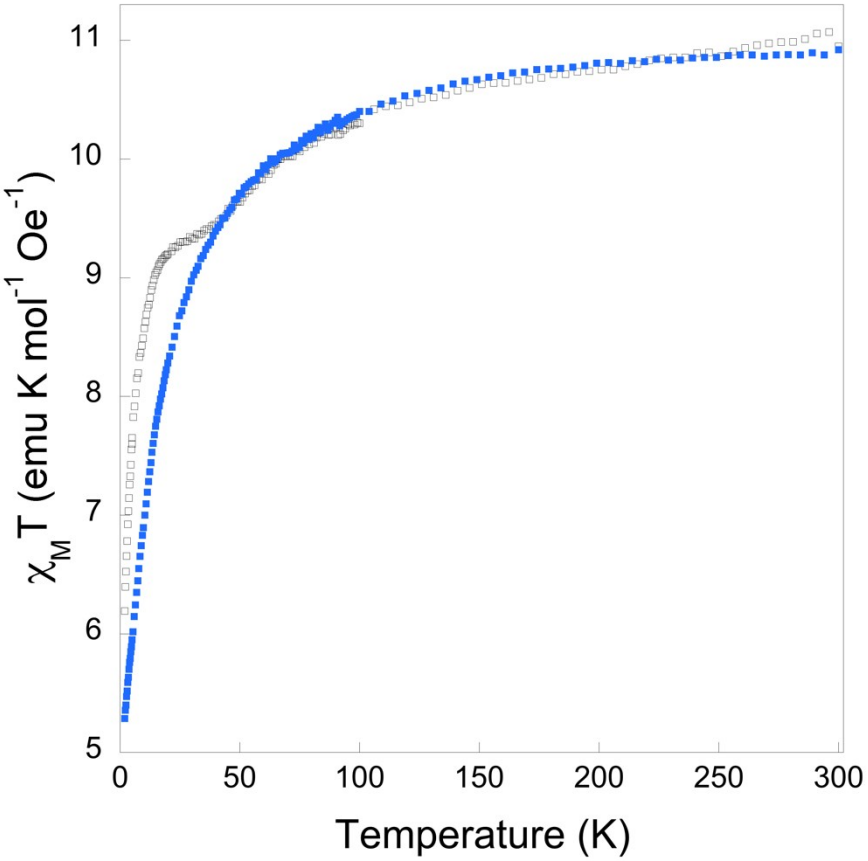

Fig. S13: Plot of $\chi_M T$ versus temperature for $[(CH_3)_2NH_2]Er(HCO_2)_2(C_2O_4)$ with ZFC and FC data shown as hollow black and filled blue markers, respectively.

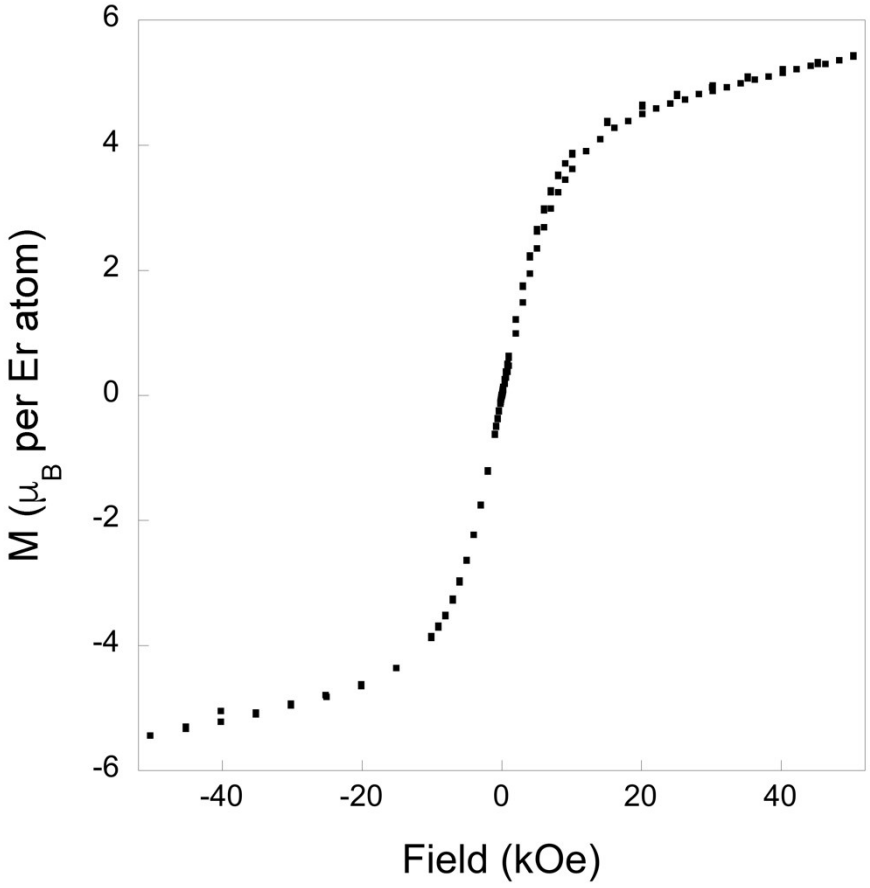

Fig. S14: Plot of magnetisation versus applied field for $[(CH_3)_2NH_2]Er(HCO_2)_2(C_2O_4)$ at 2 K.

1 CrysAlisPro Software system, version 1.171.38.43, Rigaku Oxford Diffraction, 2018.
2 G. M. Sheldrick, *Acta Crystallogr. Sect. A*, 2015, **71**, 3–8.
3 L. J. Bourhis, O. V Dolomanov, R. J. Gildea, J. A. K. Howard and H. Puschmann, *Acta Crystallogr. Sect. A*, 2015, **71**, 59–75.
4 G. M. Sheldrick, *Acta Crystallogr. Sect. C*, 2015, **71**, 3–8.
5 O. V Dolomanov, L. J. Bourhis, R. J. Gildea, J. A. K. Howard and H. Puschmann, *J. Appl. Crystallogr.*, 2009, **42**, 339–341.
6 B. A. Hunter and C. J. Howard, *A computer program for Rietveld analysis of X-ray and neutron powder diffraction patterns*, 1998.